

© IEEE. Personal use of this material is permitted. However, permission to reprint/republish this material for advertising or promotional purposes or for creating new collective works for resale or redistribution to servers or lists, or to reuse any copyrighted component of this work in other works must be obtained from the IEEE.

This material is presented to ensure timely dissemination of scholarly and technical work. Copyright and all rights therein are retained by authors or by other copyright holders. All persons copying this information are expected to adhere to the terms and constraints invoked by each author's copyright. In most cases, these works may not be reposted without the explicit permission of the copyright holder.

PRNU-based finger vein sensor identification: On the effect of different sensor croppings

Dominik Söllinger*, Babak Maser* and Andreas Uhl
University of Salzburg
Jakob-Haringer-Str. 2, 5020 Salzburg, Austria
uhl@cosy.sbg.ac.at

Abstract

In this work, we study the applicability of PRNU-based sensor identification methods for finger vein imagery. We also investigate the effect of different image regions on the identification performance by looking at five different croppings with different sizes. The proposed method is tested on eight publicly available finger vein datasets. For each finger vein sensor a noise reference pattern is generated and subsequently matched with noise residuals extracted from previously unseen finger vein images. Although the final result strongly encourages the use of PRNU-based approaches for sensor identification, it can also be observed that the choice of image region for PRNU extraction is crucial. The result clearly shows that regions containing biometric trait (varying content) should be preferred over background regions containing non-biometric trait (identical content).

1. Introduction

Biometric systems, which utilize a human's physical or behavioral characteristic, have become more and more popular in the last decades. Not only, do companies or governmental organizations rely on biometric technology to secure their environment, also everyday technology (e.g. smartphones, laptops, entrance systems) uses it extensively. Nevertheless, biometric traits also set new challenges in terms of maintaining security and integrity of biometric data. While the key material used in traditional authentication methods like PINs, passwords, smart-cards etc. can usually be changed, a person's biometric trait usually remains stable. Therefore, once biometric features are leaked, stolen or adopted many different attack scenarios become conceivable.

The fact that certain biometric modalities, e.g. fingerprints or faces, even cannot be considered as being secret simply due to their pure nature, requires researchers to come up with new strategies to detect and prevent, for instance, spoofing attacks. Attackers can easily take high-resolution images of a person's face or even fingerprints can be covertly lift off a person's glass.

Different strategies have been proposed to circumvent some of these attacks. Liveness detection has been suggested as a strategy to cope with attackers who try to fool the sensor with prerecorded data. Encryption has been proposed to secure the communication channel between sensor and feature extractor which might be intercepted and resubmitted by changed or replayed data. However, the "public" nature of aforementioned modalities simply raises the question whether ensuring the privacy of biometric data is still necessary and appropriate. Instead, the senders (sensors) identity could be directly verified as a part of the entire authentication mechanism.

At this point, passive media security techniques come into play, typically termed as "digital image forensics" [1]. A technique for sensor identification [2] is based on the so-called photo-response non-uniformity (PRNU). PRNU is often considered to be a *digital hardware fingerprint* primarily caused by pixel non-uniformity (PNU). PNU is an intrinsic property of every digital sensor caused by different sensitivity of pixels to light due to inhomogeneity of silicon wafers and imperfections during the sensor manufacturing process.

Previous work already showed that PRNU-based approaches are well-suited for sensor identification in the context of fingerprint [3] and iris [4, 5, 6, 7, 8] images. However, some work [9, 10] in the context of iris images also reported considerably fluctuating equal error rates and thresholds dependent on the sensor. This strongly motivates further research in this field.

*Both authors contributed equally

This work is organized as follows: Section 2 gives an overview of techniques used for PRNU extraction and enhancement. Section 3 introduces the datasets, explains the different experimental settings as well as the evaluation workflow in detail. Finally, experimental results are provided in Section 4 followed by a conclusion in Section 5.

2. Methodology

To extract the PRNU fingerprint we use the method proposed by *Fridrich* in [11] which is based on maximum likelihood estimation (MLE). For each image I_i the noise residual R_i gets estimated as follows:

$$R_i = I_i - F(I_i) \quad (1)$$

$F(I_i)$ is a denoised version of the original image obtained by applying an adaptive Wiener filter in the wavelet domain. As a result, $F(I_i)$ mainly contains low frequencies. After subtracting the denoised from the original image, we obtain a high-frequency image containing the residual noise. Since the noise residual might be contaminated with undesired artifacts often referred as non-unique artifacts (NUAs) [12] two different enhancement techniques are applied. Both enhancement techniques are described in Section 2.2. Finally, a maximum likelihood estimator [11] is used to obtain the PRNU factor \hat{K} by means of the following equation:

$$\hat{K} = \sum_{i=1}^N R_i I_i / \sum_{i=1}^N I_i^2 \quad (2)$$

\hat{K} is our zero-mean noise-like signal responsible for the PRNU and I_i corresponds to images of the same sensor with $i = 1 \dots N$ where N denotes the total number of images in the dataset.

To evaluate the similarity between the PRNU fingerprint \hat{K} and the residual noise R_I of a query image two different metrics are used: Normalized Cross Correlation (NCC) as shown in (3) and Peak Correlation Energy (PCE) as shown in (5).

$$NCC(X, Y) = \frac{\sum_{i=1}^W \sum_{j=1}^H \left((X(i, j) - \bar{X}) \cdot (Y(i, j) - \bar{Y}) \right)}{\|X - \bar{X}\| \cdot \|Y - \bar{Y}\|} \quad (3)$$

The presence of the PRNU fingerprint in the query image I_Q can be estimated by measuring the correlation between the noise residual R_{I_Q} of a query image I_Q and the PRNU factor \hat{K} weighted by the image content of I_Q as shown in (4).

$$\rho_{\{R_I, I_Q \hat{K}\}} = NCC(R_I, I_Q \hat{K}) \quad (4)$$

Peak Correlation Energy [13] is an alternative measure to

attenuate the influence of periodic noise contamination. It has been shown to yield more stable results in scenarios where images have been geometrically transformed and scaled [14]. Although, Kang *et al.* [15] showed that PCE may increase the false-positive rate if images have not been geometrically transformed, we still test PCE as a second metric in this work.

As in this work only image patches of the same size are compared. Image transformations like scaling and cropping are not taken into account. Consequently, the formula for PCE simplifies as follows [16]:

$$PCE = \frac{CNCC(0, 0)^2}{\frac{1}{WH - |A|} \sum_{i, j \neq A} CNCC(i, j)^2} \quad (5)$$

$CNCC$ is the circular normalized cross correlation between R_{I_Q} and $I_Q \hat{K}$. A is a small area around the peak located at position $(0, 0)$ and $|A|$ represents the cardinality of the area.

$$CNCC(x, y) = \frac{1}{WH} \sum_{i=1}^W \sum_{j=1}^H (X(i, j) - \bar{X}) \cdot (Y_{(i, j) \oplus (x, y)}(i, j) - \bar{Y}) \quad (6)$$

For both methods, NCC as well as PCE, our goal is to detect whether an image has been obtained from a certain sensor. This classification can be achieved by comparing the calculated NCC or PCC score to a pre-defined threshold τ . If the score is greater than τ we consider the query image I_Q as being obtained by the sensor.

$$\text{FromSensor}(I_Q) = \begin{cases} \text{True} & \text{if } \text{Score}(R_{I_Q}, I_Q \hat{K}) > \tau \\ \text{False} & \text{if } \text{Score}(R_{I_Q}, I_Q \hat{K}) \leq \tau \end{cases} \quad (7)$$

2.1. Wavelet-based residual extraction

Low-pass filters applied in Wavelet domain [17] have been shown to be a well-suited tool for image denoising and residual extraction. This denoising is typically achieved by applying a Wiener filter like attenuation on high-frequency sub-bands (incl. local variance estimation). Subtraction of the denoised image from the original image as shown in (1) then returns a high-frequency signal containing the residual noise.

The required steps to extract the residual can be summarized as follows:

1. Apply 4-Level Wavelet decomposition using Daubechies 8-tap WMF. Coefficients in the horizontal, vertical and diagonal high-frequency sub-bands are denoted $v(i, j)$, $h(i, j)$ and $d(i, j)$.

- For each sub-band: Estimate the local variance by applying local MAP estimation using different window sizes W where $W \in \{3, 5, 7, 9\}$.

$$\hat{\sigma}_w^2(i, j) = \max \left[0, \frac{1}{W^2} \sum_{(i, j) \in N} h^2(i, j) - \sigma_0^2 \right] \quad (8)$$

Choose the minimum local variance as final estimate:

$$\hat{\sigma}^2(i, j) = \min [\sigma_3^2(i, j), \sigma_5^2(i, j), \sigma_7^2(i, j), \sigma_9^2(i, j)] \quad (9)$$

- Obtain the coefficients for the residual noise by subtraction of the original with the denoised version. This can be easily done by setting the coefficients of the low-frequency sub-band (LL) to 0. The remaining coefficients are calculated as follows:

$$C_{Res}(i, j) = C(i, j) \frac{\sigma_0^2}{\sigma^2(i, j) + \sigma_0^2} \quad (10)$$

Note: $\sigma_0 = 3$ has been chosen empirically.

- Transform the extracted noise residual C_{Res} back to spatial domain using the inverse wavelet transform.

2.2. Enhancement Techniques

In this work we applied two different post-processing techniques to further improve the extracted residual and PRNU fingerprint.

Wiener filter: Noise residuals might be contaminated with undesired artifacts. A Wiener filter [13] applied in the frequency domain can help to suppress these artifacts.

Zero-Mean filter: Noise residuals might also be contaminated with non-unique artifacts (NUAs) introduced by demosaicing algorithms that depend on the CFA (Color Filter Array). Zero-mean filtering as proposed in [13] allows to remove these periodic artifacts.

3. Experimental Design

3.1. Datasets

In this work we evaluated the performance of our finger vein sensor identification on the following publicly available datasets. Out of each dataset a subset of 120 images has been chosen.

- **SDUMLA-HMT (SDUMLA)** - Images of the dataset [18] are stored in BMP format with 320×240 pixels in size. The selected subset is composed of images from the first 20 individuals.

- **IDIAP VERA (IDIAP-REAL)** - Images of the dataset [19] are stored in PNG format with a size of 250×665 . We have taken 120 images of the first 60 individuals out of the IDIAP-REAL sub-dataset.
- **FV-USM** - Images of the dataset [20] are stored in JPEG format with a size of 480×640 . The selected subset is composed of images from the first 30 individuals.
- **MMCBNU_6000 (MMCBNU)** - Images of the dataset [21] are stored in BMP format with a size of 640×480 . The selected subset is composed of images from the first 20 individuals.
- **PLUS-FV3-Laser-Palmar (Palmar)** - Images of the dataset [22] are stored in PNG format with a size of 600×1024 . The selected subset is composed of images from the first 20 individuals.
- **THU-FVFDV** - Images of the dataset [22] are stored in PNG format with a size of 600×1024 . The selected subset is composed of images from the first 20 individuals.
- **UTFVP** - Images of the dataset [23, 24] are stored in PNG format with a size of 672×380 . The selected subset is composed of images from the first 20 individuals.
- **HKPU-FV** - Images of the dataset [25] are stored in BMP format with a size of 513×256 . The selected subset is composed of images from the first 60 individuals.

3.2. Image Preprocessing

Images are part of THU-FVDT and PLUS-FV3-Laser-Palmar are provided in portrait orientation. To align them with images of the remaining datasets, all images of these two datasets were rotated by 90° .

3.3. Experimental Settings

The primary goal of this work is to not only study the general applicability of PRNU-based sensor identification for finger vein images but also investigate the effect of different croppings on the identification performance. We assume that fingerprints generated from uncorrelated data in order to facilitate the out-averaging of image-content related high-frequency content are better suited for sensor identification than fingerprints generated from correlated data. As a result, we expect bad performance for fingerprints generated based on regions containing non-biometric trait (typically background regions) since only illumination fluctuations might lead to differences in such regions. On the other hand, we expect good performance for regions containing biometric trait due to a better variability of the

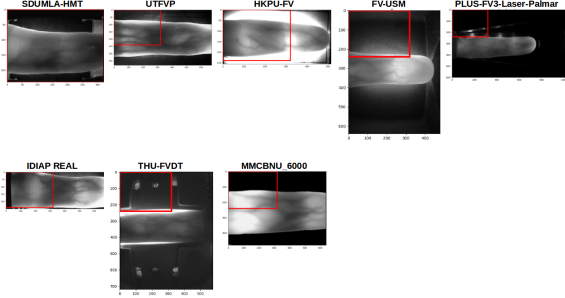


Figure 1: Sample Patches: Top-left

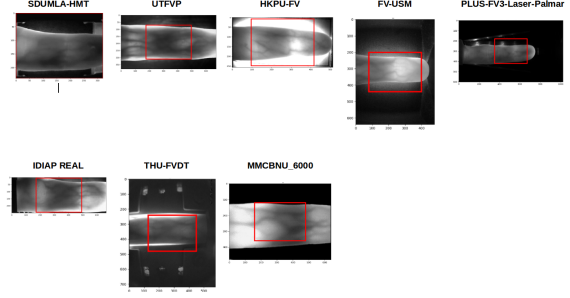


Figure 2: Sample Patches: Center 320×240

image content.

To verify whether this assumption holds, we compare the identification performance of five different cropping modes. Each mode extracts sample patches with a fixed size at a fixed position in the image. Consequently, the characteristics of images also differ significantly from each other.

The following list provides an intuition for the choice of different cropping modes and the image characteristics:

- **Background 320×100 :** Two concatenated image slices (320×50) taken from the top and bottom region of an image. As shown in Figure 5 the background region exclusively contains non-biometric trait.
- **Center 320×100 :** 320×100 image region taken from the center. The patch size and region was chosen to exclusively contain biometric trait (finger vein texture). (Figure 4)
- **Center 320×150 :** 320×150 image region taken from the center. Still image patches mainly contain biometric trait. However, also non-biometric trait is contained in case of some datasets (e.g. SDUMLA-HMT). (Figure 3)
- **Center 320×240 :** 320×240 image region taken from the center. The choice of this patch size is motivated by low resolution images. Patch sizes beyond 320×240 would require image padding for certain images and therefore bias the classification. Since the patch is taken from the center, image patches always contain biometric trait. The amount of non-biometric is dependent on the dataset's image size. (Figure 2)
- **Top-Left 320×240 :** For comparison we also extract another 320×240 -sized image region from the top-left corner. Due to its location, the image patch is guaranteed to contain non-biometric trait as well as a large amount of biometric-trait for some datasets. (Figure 1)

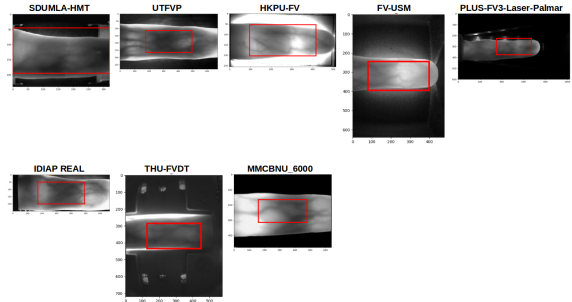


Figure 3: Sample Patches: Center 320×150

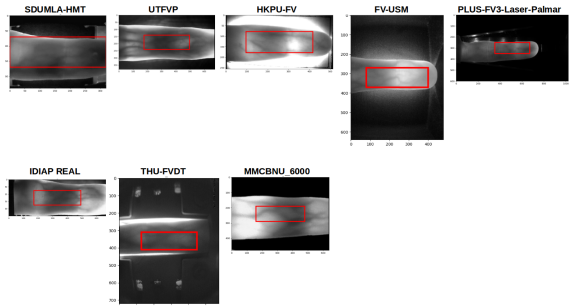


Figure 4: Sample Patches: Center 320×100

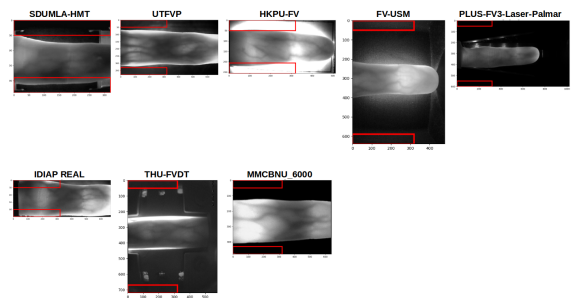


Figure 5: Sample Patches: Background

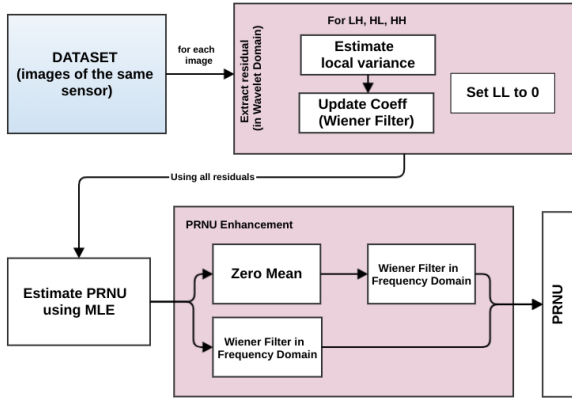


Figure 6: PRNU Estimation Workflow

3.4. Evaluation Workflow

This section provides a detail step-by-step explanation of the PRNU estimation and the performance evaluation process. First of all, to reliably assess the performance of the PRNU-based sensor identification technique, *subjectwise* 4-fold cross validation is applied. In each fold 90 images are used to estimate the sensor’s PRNU. Thus, the testing set is composed of 960 images taken from the remaining datasets and 30 images belonging to the sensor used for PRNU estimation. This immediately indicates that the testing set is heavily biased towards outliers (samples not obtained by the sensor). Since the AUC-ROC is not well-suited for imbalanced datasets, we also report AUC-Precision-Recall which is better suited for imbalanced datasets.

PRNU Estimation:

Figure 6 illustrates the different steps taken in the PRNU estimation phase. It is important to note that enhancement is only applied on the estimated (final) PRNU fingerprint. The residual images itself are not further enhanced. A detailed description of the residual extraction and PRNU enhancement process is provided in Section 2.

Residual Extraction:

The residual extraction workflow is illustrated in Figure 7. In fact, the workflow is similar to the PRNU estimation process. However, residual enhancement is directly applied on each individual residual image. After obtaining the PRNU fingerprint for a sensor, the performance is evaluated by extracting the residual for every image in the test set and classifying it as inlier or outlier. The similarity between the PRNU fingerprint and the query image is measured by means of NCC or PCE as explained in Section 2.

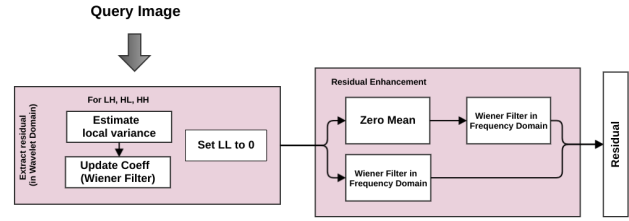


Figure 7: Residual Workflow

4. Results

In this section, we present the results obtained by using different croppings and enhancement techniques. More precisely, we are primarily interested in the following aspects:

- General applicability of PRNU-based sensor identification in the context of finger vein
- Suitability of different enhancement methods for PRNU extraction
- Effect of different croppings on the identification performance
- Suitability of different comparison metrics: PCE / NCC

To analyze the effect of different crop sizes and enhancement methods we calculate the *average* AUC scores for all sensor types. Results for each cropping and enhancement method are shown in Figure 8. Furthermore, we provide the exact results for the Wiener filter (WF) enhancement in Table 1.

4.1. Effect of different enhancement methods

As we can see in Figure 8, Wiener filtering (WF) provides the best overall result. Figure 8a and 8b show that only in the TOP-LEFT case, not applying any enhancement works best. Furthermore, it can be observed that Zero-Mean filtering should be avoided. Independent of the cropping, the AUC score starts to decrease once Zero-Mean filtering is applied. An effect obviously caused by the fact that most finger vein sensors do not use color filter arrays (CFAs).

4.2. Effect of similarity measure

As shown in Table 1, both similarity measures (NCC / PCE) in most cases exhibit a similar identification performance. Although we are not able to identify a clear winner among both measures, the use of NCC seems to be more appealing due to its low algorithm complexity.

4.3. Effect of different croppings

As can be seen in Figure 1 - 5 choosing location and size of the crop region is a crucial task when it comes to extracting real biometric trait out of finger vein images. Therefore, as discussed in Section 3.3, for a better understanding

	NCC AUC- ROC	NCC AUC- Precision- Recall	PCE AUC- ROC	PCE AUC Precision- Recall
CENTER 320×240	0.992	0.978	0.991	0.973
CENTER 320×150	0.998	0.979	0.997	0.978
CENTER 320×100	0.996	0.953	0.994	0.956
BACKG. 320×100	0.886	0.627	0.859	0.547
TOP-LEFT 320×240	0.978	0.968	0.993	0.960

Table 1: Average AUCs for different croppings + Wiener Filter (WF)

of the impact of different croppings on the identification performance we tested our identification algorithm using five different croppings. Again, it should be emphasized that the background cropping is chosen in a way that it only contains non-biometric trait while the smallest center cropping only contains biometric trait. Remaining regions contain a mixture of both traits. Note that, the background cropping and the smallest center cropping (320×100) have the same size and therefore carry the same amount of information.

In Figure 8 (a-d) we observe that the performance of CENTER (320×100) clearly outperforms the performance of the background cropping as the background region mainly contains identical content while the center cropping contains varying content (typically biometric trait). The effect of larger, mixed regions can be studied by looking at the center croppings 320×150 as well as 320×240. Obviously, due to their larger size, these new croppings can contain more biometric trait as well as non-biometric trait. As we can see in Table 1 the cropping CENTER (320×150) exhibits the best identification performance among all five croppings regardless of the similarity measure. Furthermore, it can be seen that increasing of the crop size does not necessarily improve the identification performance. For instance, the center crop size 320×240 does not achieve the highest identification performance. This might be due to the fact that increasing crop sizes also add more background parts to the estimated fingerprint.

4.4. Sensor comparison with different croppings

In this section, we investigate the impact of image acquisition on the sensor identification performance. Therefore, we analyze the effect of three different croppings

(BACKGROUND [320×100], CENTER [320×100], CENTER [320×150]) on the identification performance for each individual sensors.

In Figure 9 (a-d) we can see a poor identification performance for background regions for MMCBNU, PALMAR, THU-FVFDT and FV-USM. Obviously, since the background regions mainly contain identical content, hardly any PRNU information can be extracted. This effect could be due to the physical characteristics (design) of the sensor apparatus or image preprocessing. Once a sensor is placed inside an enclosed chamber, the surrounding area of a finger will be almost uniform black.

Figure 9a shows AUC ROC scores for different sensors using the NCC similarity measure. Both center croppings are substantially superior to the background cropping except for THU-FVFDT. In particular, the results for MMCBNU and PALMAR background croppings can be considered as extremely bad.

A similar scenario can be observed in Figure 9c. AUC ROC scores (PCE) for the background cropping for PALMAR and THU-FVFDT are dramatically inferior to other center croppings. Classification for MMCBNU background although works significantly better than when using NCC. For the remaining sensors in Figure 9c we see absolute and perfect superiority of center croppings.

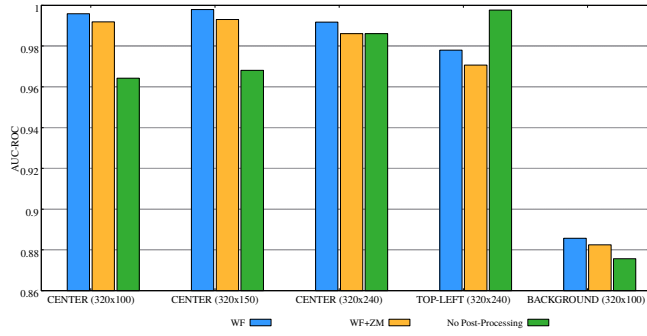
In Figure 9b, the result shows low AUC-Precision-Recall scores for all sensor in case of background croppings.

In Figure 9d, absolute superiority of the center croppings and inferiority of the background cropping for all types of sensors can be observed as well.

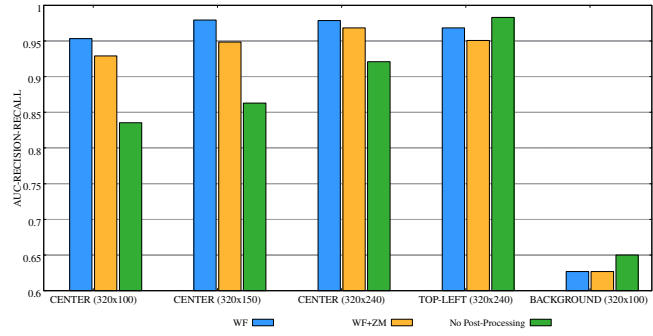
Consequently, we can conclude that regardless of the applied similarity measures (NCC/PCE) or enhancement techniques the most striking features of Figure 9 (a-d) are inferiority of the background cropping and superiority of the center croppings for most of the sensors.

5. Conclusion

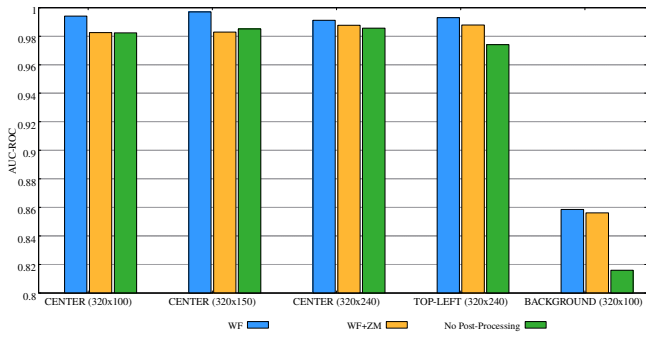
This work studied the applicability of PRNU-based identification methods for different finger vein crop sizes. The results clearly demonstrated that PRNU-based algorithms are well-suited for sensor identification in the context of finger vein images. Furthermore, it confirmed the assumptions that PRNU fingerprints should be generated from uncorrelated data. While regions containing biometric trait (uncorrelated data) could be classified perfectly, background regions containing non-biometric trait (correlated data) turned out to be problematic. The experiments also indicated that Zero-Mean filtering should be avoided when working with finger vein images. By contrast, Wiener filtering turned out to be a good enhancement technique in the context of finger vein sensor identification.



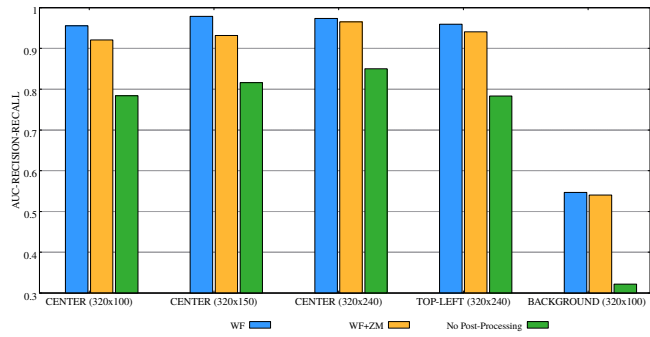
(a) AVG AUC ROC for NCC



(b) AVG AUC Precision-Recall for NCC

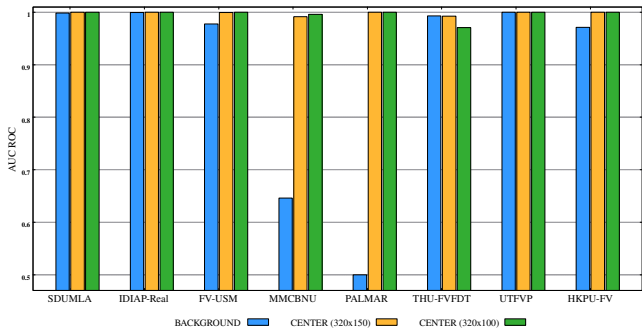


(c) AVG AUC ROC for PCE

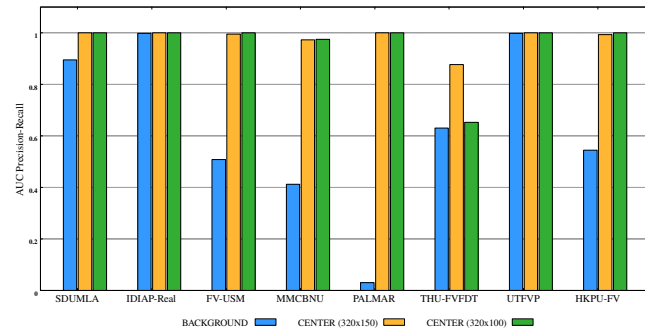


(d) AVG AUC Precision-Recall for PCE

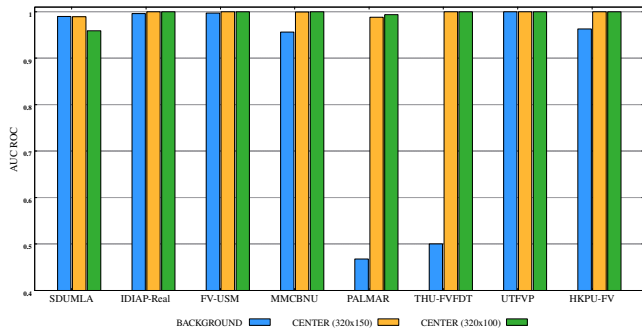
Figure 8: Average AUCs for different croppings and filters



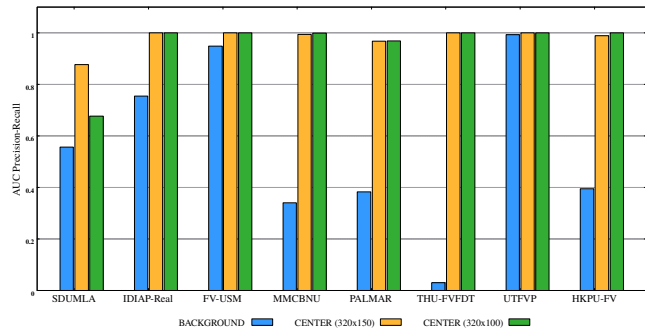
(a) AUC ROC for NCC



(b) AUC Precision-Recall for NCC



(c) AUC ROC for PCE



(d) AUC Precision-Recall for PCE

Figure 9: AUCs clustered by sensor

References

- [1] H. Farid. Image forgery detection. *IEEE Signal Processing Magazine*, 26(2):16–25, March 2009.
- [2] Jan Lukas, Jessica Fridrich, and Miroslav Goljan. Digital camera identification from sensor pattern noise. *IEEE Transactions on Information Forensics and Security*, 1(2):205–214, 2006.
- [3] Nick Bartlow, Nathan Kalka, Bojan Cukic, and Arun Ross. Identifying sensors from fingerprint images. In *Computer Vision and Pattern Recognition Workshops, 2009. CVPR Workshops 2009. IEEE Computer Society Conference on*, pages 78–84. IEEE, 2009.
- [4] Francesco Marra, Giovanni Poggi, Carlo Sansone, and Luisa Verdoliva. A deep learning approach for iris sensor model identification. *Pattern Recognition Letters*, 113:46–53, 2018.
- [5] Luca Debiasi and Andreas Uhl. Blind biometric source sensor recognition using advanced prnu fingerprints. In *Signal Processing Conference (EUSIPCO), 2015 23rd European*, pages 779–783. IEEE, 2015.
- [6] Christof Kauba, Luca Debiasi, and Andreas Uhl. Identifying the origin of iris images based on fusion of local image descriptors and prnu based techniques. In *Biometrics (IJCB), 2017 IEEE International Joint Conference on*, pages 294–301. IEEE, 2017.
- [7] Luca Debiasi, Christof Kauba, and Andreas Uhl. Identifying iris sensors from iris images. *Iris and Periocular Biometric Recognition*, 5:359, 2017.
- [8] Susan El-Naggar and Arun Ross. Which dataset is this iris image from? In *WIFS*, pages 1–6, 2015.
- [9] Nathan Kalka, Nick Bartlow, Bojan Cukic, and Arun Ross. A preliminary study on identifying sensors from iris images. In *Proceedings of the IEEE Conference on Computer Vision and Pattern Recognition Workshops*, pages 50–56, 2015.
- [10] Andreas Uhl and Yvonne Höller. Iris-sensor authentication using camera prnu fingerprints. In *Biometrics (ICB), 2012 5th IAPR International Conference on*, pages 230–237. IEEE, 2012.
- [11] Jessica Fridrich. Digital image forensics. *IEEE Signal Processing Magazine*, 26(2), 2009.
- [12] Thomas Gloe, Stefan Pfennig, and Matthias Kirchner. Unexpected artefacts in prnu-based camera identification: a dresden image database case-study. In *Proceedings of the on Multimedia and security*, pages 109–114. ACM, 2012.
- [13] Jessica Fridrich. Sensor defects in digital image forensic. In *Digital Image Forensics*, pages 179–218. Springer, 2013.
- [14] Miroslav Goljan and Jessica Fridrich. Camera identification from cropped and scaled images. In *Security, Forensics, Steganography, and Watermarking of Multimedia Contents X*, volume 6819, page 68190E. International Society for Optics and Photonics, 2008.
- [15] Xiangui Kang, Yinxiang Li, Zhenhua Qu, Jiwu Huang, et al. Enhancing source camera identification performance with a camera reference phase sensor pattern noise. *IEEE Transactions on Information Forensics and Security*, 7(2):393–402, 2012.
- [16] Xufeng Lin and Chang-Tsun Li. Preprocessing reference sensor pattern noise via spectrum equalization. *IEEE Transactions on Information Forensics and Security*, 11(1):126–140, 2016.
- [17] M Kivanc Mihcak, Igor Kozintsev, and Kannan Ramchandran. Spatially adaptive statistical modeling of wavelet image coefficients and its application to denoising. In *Acoustics, Speech, and Signal Processing, 1999. Proceedings., 1999 IEEE International Conference on*, volume 6, pages 3253–3256. IEEE, 1999.
- [18] Y. Yin, L. Liu, and X. Sun. SDUMLA-HMT: A Multimodal Biometric Database. In *The 6th Chinese Conference on Biometric Recognition (CCBR 2011)*, volume 7098 of *Springer Lecture Notes on Computer Science*, pages 260–268, 2011.
- [19] Pedro Tome, Matthias Vanoni, and Sébastien Marcel. On the vulnerability of finger vein recognition to spoofing. In *IEEE International Conference of the Biometrics Special Interest Group (BIOSIG)*, September 2014.
- [20] M. S. M. Asaari and B. A. Rosdi S. A. Suandi. Fusion of band limited phase only correlation and width centroid contour distance for finger based biometrics. *Expert Systems with Applications*, 41(7):3367–3382, 2014.
- [21] Yu Lu, Shan Juan Xie, Sook Yoon, Zhihui Wang, and Dong Sun Park. An available database for the research of finger vein recognition. In *Image and Signal Processing (CISP), 2013 6th International Congress on Image and Signal Processing (CISP 2013)*, volume 1, pages 410–415. IEEE, 2013.
- [22] Christof Kauba, Bernhard Prommegger, and Andreas Uhl. Focussing the beam - a new laser illumination based data set providing insights to finger-vein recognition. In *Proceedings of the IEEE 9th International Conference on Biometrics: Theory, Applications, and Systems (BTAS2018)*, pages 1–9, Los Angeles, California, USA, 2018.
- [23] Pedro Tome, Matthias Vanoni, and Sébastien Marcel. On the vulnerability of finger vein recognition to spoofing attacks. In *Proceedings of the International Conference of the Biometrics Special Interest Group (BIOSIG'14)*, pages 111–120, September 2014.
- [24] B.T. Ton and R.N.J. Veldhuis. A high quality finger vascular pattern dataset collected using a custom designed capturing device. In *International Conference on Biometrics, ICB 2013*. IEEE, 2013.
- [25] Ajay Kumar and Yingbo Zhou. Human identification using finger images. *IEEE Transactions on Image Processing*, 21(4):2228–2244, 2012.